## Universities of Leeds, Sheffield and York
## http://eprints.whiterose.ac.uk/

# The Dynamic Characterisation of Disk Geometry Particle Dampers

W Liu, G R Tomlinson and J A Rongong

Department of Mechanical Engineering, University of Sheffield

Mappin Street, Sheffield S1 3JD, UK

**Abstract**

Particle dampers (PDs) have the advantages of being simple in geometry, small in volume and applicable in extreme temperature environments. Experimental studies have shown that PDs can offer considerable potential for suppressing structural resonant conditions over a wide frequency range. In this paper, the nonlinear characters of PDs are studied experimentally in a series of response-level-controlled tests. The effect of the geometry is studied and a method is developed to model the nonlinear damping of PDs as equivalent viscous dampers that can be applied directly to engineering structures at the design stage.

# 1.    Introduction

A particle damper is a device with one or more cavities filled with dry granular solids. A particularly important aspect that contributes to the unique properties of granular materials is that the interactions between individual grains (and between grains and the container walls) are dissipative because of surface friction and the inelasticity of collisions. An overwhelming advantage of particle dampers, compared with conventional damping devices that employ viscoelastic materials, is that particle dampers can operate in extreme temperature conditions when using metallic, tungsten carbide or ceramic particles.

The behaviour of vibrating structures with particle dampers attached to them have been investigated experimentally [1], where it was shown that particle dampers are highly effective over a wide range of frequencies, resulting in several modes of vibration being damped simultaneously. There exist a large number of parameters affecting the damper performance such as: particle shapes, sizes, cavity filling fractions, material properties (viscosity, elasticity, friction coefficients and density), and cavity shape. Because of this and due to the complex interactions of the loss mechanisms in a particle damper, it is extremely difficult to define explicitly a particle damper configuration for a particular application. Instead, "rule-of-thumb" guidelines for designing particle dampers have been proposed [4].

Analytical studies require a way of modelling the properties of granular media. Over the last century, many researchers (particularly physicists) have studied the properties of granular media. However, the mechanical state of granular matter is still an open and frequently debated question. For instance, to date, there is no consensus on how

to express the macroscopic constitutive relations solely from microscopic considerations under various boundary conditions or loading histories [7].

The mechanics of granular materials is often studied by formulating the macro-behaviour in terms of micro-quantities [6], i.e. the dynamic behaviour is derived from the analysis of individual particles. In order to reduce computational effort, simplifying assumptions are frequently made. A two-dimensional analysis, based on molecular dynamics principles, has been used to study effects of frequency and amplitude on the response of a container filled with particles [3]. In this study, an effective damping parameter, which describes an equivalent linear oscillator with the same damping properties, is defined by dividing the averaged dissipated power under stationary vibration with the amplitude of input energy. More complicated models, including 3D behaviour and particle rotation have been developed [4, 5] and used simulate the response of dampers containing small numbers of particles. By solving the equations of motion of the entire set of particles at each time step, the state of the system can be obtained from a given initial condition. However, in practical applications such as the case described in reference [1], particle dampers often contain tens of thousands of particles. The prediction of the response of a structure with such a damper attached is computationally very expensive.

In contrast, experiments can reveal the collective behaviour of particle dampers more accurately. As particle dampers are easy to make and install on a structure, it is relatively simple to investigate their dynamic behaviour via controlled experiments [2]. This paper presents the results from a series of dynamic tests of particle dampers on a SDOF test-rig. The energy dissipation mechanism, which characterises the

nonlinear damping, is represented by a discrete parameter model that can be employed in the design of particle dampers.

## 2.    Dynamic Behaviour of Particle Dampers

The test-rig employed for all the experimental studies is shown in Figure 1. The rig was designed such that the first resonant frequency (246*Hz*) was well below the next measured structural resonance allowing the rig to effectively behave as a single degree of freedom (SDOF) system. The rig comprised a hollow block or mass that housed the particle damper, the block being rigidly connected to a spring (a section of a rectangular tube) which in turn was 'grounded' to a very stiff support structure.  The mass of the block was 0.780 *kg*. The stiffness of the frame spring was found (from the resonant frequency) to be $2.017 \times 10^6$ *N/m*. The SDOF system was excited in the horizontal plane by an electrodynamic exciter. The particle dampers used in the tests comprised of a steel container enclosing a cylindrical cavity. The cavity was filled to approximately 95% volume with 0.8mm diameter steel spheres, the mass of the particles being 90 grams. Controlled stepped-sine tests were carried out using SigLab, a dynamic signal analyser integrated with MATLAB. SigLab generates the stepped-sine signal which is amplified and then input into the exciter. Simultaneously, SigLab can record the response of the system which allows a controlled output response at a pre-set level via a close-loop control system to be maintained during testing.

Frequency response functions (FRFs) were measured in terms of the acceleration of the block (measured using a B&K miniature accelerometer) divided by the input force (measured using a force gauge). The frequency range of interest (220-260*Hz*) encompassed the first resonant frequency of the test-rig. The typical collective or

4

macro-dynamic behaviour of a particle damper attached to the SDOF system, presented as a set of frequency response functions, is shown in Figure 2. For these results, the diameter and depth of the cavity were $39.7mm$ and $15.9mm$ respectively. The dashed line is the FRF of the system with an empty damper – the cavity is not filled with the granular material. This FRF was found to be independent of excitation level. The FRFs, marked 1, 2, 3 and 4 were measured with the filled damper at response levels $0.1g$, $1g$, $4g$ and $8g$. It can be seen that at the very low response level (0.1g) the particles behave as an added mass, which simply causes the system's resonant frequency to drop from $246Hz$ to about $234Hz$. With the increase of the excitation level, the damping rises dramatically and the resonant frequency of the SDOF system shifts gradually towards that measured with the empty particle damper (FRF marked 11 in Figure 2). When the response level reaches $12g$ (FRF marked 5), the resonant frequency is 246Hz – the same as when the particle damper was empty. Further increases in the response level to $16g$, $20g$, $25g$, $30g$, $35g$ and $40g$ (FRFs marked 6 to 11) result in an almost unchanged resonant frequency and in reducing damping behaviour.

The dynamic behaviour of the particle dampers can be explained by the mechanism of collision and friction. The collision and friction between particles and between particles and the walls dissipate the kinetic energy of the vibrating system. When the response level is very low (>>1$g$), there is almost no relative motion between particles and between particles and the walls. There is little damping as the particle damper simply plays the role of an added mass. When the response level is close to $1g$, the inertia forces of the particles on the top (free) surface exceed the static friction forces locking them together. These particles move in the vicinities of their original

5

positions. The movement of these layers dissipates energy (via friction) producing the FRF shown as curve 2 in Figure 2, which is approximately $7dB$ lower in amplitude compared with curve 1.

As the excitation level is increased, the depth of moving particles increases with an increase in the dissipated energy. With further increases in the excitation amplitude, particles tend to roll over one another (reducing dissipated energy) until eventually all the particles in the cavity display a form of convective motion. As the amplitude is increased further, the particles display a gas-phase character [1, 3]. In the gas-phase the particle friction interaction is substantially reduced which results in an effective damping decrease. This can been seen in Figure 2, when the response levels are above $12g$ (curves 5 to 11).

It is interesting to note that there appears to be a stick-slip friction mechanism present that depends on the frequency of excitation. In Figure 2, at very low ($\leq 1g$) or very high ($> 20g$) acceleration response levels, where the friction mechanism does not dissipate significant vibration energy, the FRF curves are relatively smooth. For response levels between $1g$ and $20g$, the FRF curves display fluctuations. A typical FRF, at a response level of $8g$, is shown in Figure 3. The stick-slip process is denoted by points A-B-C on the FRF. From A to B, clusters of particles display no relative motion until the slip process starts at frequency B. When slip occurs, the particles are activated and the level of the FRF drops to C. The process is continuously repeated as the frequency of the excitation changes which results in fluctuations appearing in the FRF as shown in Figure 3. This process was independent of the sequence of the tests in that several tests were repeated, with the same

6

configuration, and exactly the same phenomena were observed.

## 3.    Particle Dampers with Geometry Variations

The performance of a particle damper depends on several parameters. One of the crucial parameters is the cavity geometry. With the same size, material and almost the same volume of particles, five different geometries were tested as detailed in Figure 4 and Table 1. The ratio of depth $L$ to diameter $D$ is defined as $\alpha$, $\alpha = L/D$.

The results shown in Figures 2, 5, 6, 7 and 8 correspond to particle damper geometries of $\alpha = 0.4$, 0.2, 0.6, 0.8 and 1.0 respectively. The controlled output response levels were $0.1g$, $1g$, $4g$, $8g$, $12g$, $16g$, $20g$, $25g$, $30g$, $35g$ and $40g$ respectively for these tests.

By comparing the FRFs in Figures 2, 5, 6, 7 and 8 it can be observed that the cavity geometry plays a very important role in the dynamic behaviour of particle dampers. With increasing values of $\alpha$, the transition from solid to convective (fluidisation) and then to gas-like behaviour occurs at a lower excitation level. This phenomenon can be explained in general terms by considering the relative magnitude of static and dynamic forces acting on particles at different positions in the cavity. When at rest, the pressure distribution is controlled by gravity – if one were to assume hydrostatic pressure, average normal forces at contact points would increase linearly with depth. For relative motion to occur under dynamic loading, normal and/or tangential inertia forces have to exceed the static ones locking the particles together. For example, sliding can occur where tangential forces exceed the product of the normal force and the coefficient of friction. Thus, the static pressure distribution gives an indication of

the ease with which fluidisation occurs under excitation without resorting to the calculation of the dynamic pressure (and hence contact condition), by for example using the Discreet Element Method [5]. A simple, approximate assessment method, such as the consideration of static pressure, is of particular value in the design of dampers where large numbers of particles (well in excess of 5000 particles for the dampers considered in this paper) make the DEM method computationally very demanding.

In a contained granular medium, static pressure does not increase hydrostatically. One of the simplest models is Jansen's [6] for a cylindrical container containing particles that has its polar axis parallel to the gravitational field. In this approach, a single parameter is $K$ used to describe the way in which the stress field of the particles tends to be redirected perpendicularly to the initial load [6]. In the configuration used in the experiments described in this paper, the polar axis of the cylinder is horizontal and so a modification to Jansen's model is required.

Figure 9 shows the model for the pressure distribution analysis. The equilibrium condition in the vertical direction for the particular slice of particles is,

$$Adp_v + F_1 + F_2 = \rho\phi gAdh \tag{1}$$

in which the surface area $A = 2xL$, $\rho$ is the mass density of a particle and $\phi$ the volume fraction, $F_1$, $F_2$ are the friction force on the straight walls and the circular wall respectively.

$$F_1 = 4\mu_s Kp_v xdh \tag{2}$$

$$F_2 = 2L\mu_s K p_v \sin\alpha \cdot dh \tag{3}$$

In these equations $\mu_s$ is the static friction coefficient between grains and walls and $K$ is the Janssen parameter or coefficient of redirection toward the wall of the vertical stress applied to the material [6]. Substituting equation (2) and (3) into (1) gives,

$$\frac{dp_v}{dh} + \mu_s K \left( \frac{2}{L} + \frac{1}{R} \right) p_v = \rho\phi g \tag{4}$$

Let $\dfrac{1}{R_e} = \dfrac{1}{L} + \dfrac{1}{2R}$ then (4) becomes

$$\frac{dp_v}{dh} + \frac{2\mu_s K}{R_e} p_v = \rho\phi g \tag{5}$$

which can be rewritten as,

$$\frac{d}{dh}\left[ \exp\left( \frac{2\mu_s K}{R_e} h \right) p_v \right] = \rho g \exp\left( \frac{2\mu_s K}{R_e} h \right) \tag{6}$$

Integrating equation (6) gives,

$$p_v \exp\left( \frac{2\mu_s K}{R_e} h \right) = \frac{\rho\phi g R}{2\mu_s K} \exp\left( \frac{2\mu_s K}{R_e} h \right) + C \tag{7}$$

where $C$ is a constant to be determined from the initial conditions. If one assumes the initial pressure on the top of the structure is $p_{v0}$, then the constant $C$ is,

$$C = p_{v0} - \frac{\rho\iota g R}{2\mu_s K} \tag{8}$$

9

and (7) becomes

$$p_v = \frac{\rho \phi g R_e}{2 \mu_s K}\left[1 - \exp\left(-\frac{2\mu_s K}{R_e}h\right)\right] + p_{v0}\exp\left(-\frac{2\mu_s K}{R_e}h\right) \tag{9}$$

It is noticed that an equivalent cylindrical Janssen model to equation (9) exists which has a radius $R = R_e$.

If the parameters in equation (9) are assumed to be $\mu_s = 0.74$ (steel to steel), $K = 0.7$ (suggested by [7]), $\rho = 7.8 \, grams/cm^3$, $\phi = 0.58$ (measured) and $p_{v0} = 0$ (particles are in equilibrium under their own weight), then for the five particle dampers with different $\alpha$ - values, a group of curves, $p_v$ versus $h$ can be drawn according to expression (9). This is shown in Figure 10.

The curves show that the static pressure $p_v$ saturates exponentially with depth $h$. Pressure saturation occurs because contact point friction allows the medium to carry shear loads in the vertical plane. At saturation pressure, the weight of a layer of particles is supported by the side walls by this mechanism, thus further increases in pressure do not occur [6]. For the damper geometries considered, saturation occurs at a depth of approximately $20mm$ when $\alpha = 0.2$ and $30mm$ when $\alpha = 0.4$. Where $\alpha = 0.6$ and above, saturation does not occur in the dampers and peak pressures are up to 50% higher. Initially, this might seem to disagree with the hypothesis that increased static pressure reduces the ease with which fluidisation occurs. However, it is important to remember that the dampers have circular cross-section so that there are different numbers of particles at different depths. Also, for a given excitation force, the instantaneous dynamic pressure varies from damper to damper because of the

change in cross-sectional area. Two parameters are used here to compare the ease of fluidisation between dampers. The first is the static pressure normalised by cross sectional area,

$$p_{norm} = p_{static} \left( \frac{R_n}{R_0} \right)^2 \qquad (10)$$

where $R_n$ and $R_0$ are the radii of the baseline and $n^{th}$ dampers respectively. This is a measure of the forces stopping the particles from fluidising. The second is $N_p$ the number of particles in the damper that are below a given static pressure – indicative of the number of particles that fluidise at a given excitation level. For the dampers considered, using the condition $\alpha = 1$ as the baseline, a plot showing these parameters is presented in Figure 11. It can be seen from this plot that the low diameter dampers (large $\alpha$) contain a greater number of particles at low pressure making them easier to fluidise. This can clearly be seen from the experimentally obtained FRFs in Figure 2, 5, 6, 7 and 8.

## 4.    An Equivalent Viscous Damping Model

The model used to represent the experimental system is shown in Figure 12. The effective mass of the particles is denoted by $m_p$ and the nonlinear damping is denoted by $c_{eq}$. Since the mass $m_0$ (mass of the block) and stiffness $k$ of the system are known, the equivalent viscous damping coefficient $c_{eq}^{(i)}$ for the $i^{th}$ response level can be obtained from

$$c_{eq}^{(i)} = 2\varsigma_i \sqrt{km_i} \qquad (11)$$

11

in which $\varsigma_i$ is identified by curve fitting to the measured FRF and $m_i = m_0 + m_p$. The

discrete nonlinear damping coefficient of the particle damper $c_{eq}(v)$, as a function of

velocity, can be expressed as a continuous function by fitting a curve to the equivalent

viscous damping coefficients $c_{eq}^{(i)}$, $i = 1, 2, ..., n$ as shown in Figure 13.

In this example, the curve fitting function is based on the Gamma distribution

function in probability [9],

$$c_{eq}(v) = \frac{A}{\beta \Gamma(\gamma)} \left( \frac{v - \mu}{\beta} \right)^{\gamma-1} e^{-\frac{v-\mu}{\beta}} + B, \text{ with } v \geq \mu, \text{ and } \beta, \gamma > 0 \tag{12}$$

in which $\gamma$ is the shape parameter, $\mu$ is the location parameter, $\beta$ is the scale

parameter, and $\Gamma$ is the gamma function which has the formula ,

$$\Gamma(a) = \int_0^\infty t^{a-1} e^{-t} dt \tag{13}$$

Shape parameters allow the function to take on a variety of shapes. A location

parameter simply shifts the graph left or right on the horizontal axis. The effect of the

scale parameter is to stretch out the graph. Parameter $A$ is designated to adjust the gain

and parameter $B$ is the constant to which the function converges. The asymptotic

property of the damping dynamic behaviour is clearly described by the function. To

obtain the parameters, an optimisation problem was constructed using,

$$\min_v \frac{1}{2} \sum_i \left( c_{eq}(v_i) - c_{eq}^{(i)} \right)^2 \tag{14}$$

The parameters are obtained by solving the nonlinear Least Squares problem. The

curve-fitted results to the discrete values of the $c_{eq}^{(i)}$, $i = 1, 2, ..., n$, are shown in

Figure 13. The parameters obtained from nonlinear optimisation implementations are listed in Table 2.

It should be noticed that the restriction in the velocity range, $v \geq \mu$, in equation (11) indicates that the model does not cover the low velocity range, $0 < v < \mu$. In practice, however, it is only the relatively high response levels of the particle dampers that is of concern and the absence of the predictions at low velocities does not significantly affect the application of the model. As shown in Figure 13, the nonlinear damping coefficient in the range $0 < v < \mu$ can be estimated approximately by linear extrapolation.

The functions described by equation (11) can then be used in a Finite Element model for prediction purposes.

## 5. Conclusions

The dynamic behaviour of disc-geometry particle dampers has been characterised. It has been shown that the damping is strongly dependent on the response level. A stick-slip process was observed from the FRFs measured at various response levels, which reveals that the vibration energy is mainly dissipated by the friction between particles and between particles and the walls of the cavity.

The effect of geometry parameters on the dynamic behaviour of particle dampers was investigated by changing the diameter and thickness of the cavity simultaneously with the volume kept constant. It has been shown that the ratio of thickness to diameter of the disk cavity plays an important role due to the different pressure distributions which in turn control the eventual motion of the particles. The static pressure

distribution of particles in a disk cavity with the polar axis horizontal was derived, yielding similar result to Janssen's model. This was used to relate the damper geometry to the ease of activation.

The nonlinear behaviour of particle dampers was characterised by an equivalent viscous damping model. The parameters in the model were estimated by solving a nonlinear least squares problem. The important parameters contributing to the nonlinear damping curve such as the peak damping and the convergence damping level are defined by a five-parameter model. The procedure of modelling the equivalent viscous damping of particle dampers by $c_{eq}(v)$ is experiment-based. It is accurate, physically meaningful and easy to implement. Compared with the studies based on the microscopic scale such as molecular dynamics or the discrete element method, it is more efficient and applicable. The model extracted can be applied to other systems with the corresponding particle damper applied at the stage of design by adding a nonlinear dashpot at the mesh point of the finite element model of the structure.

**Acknowledgements**

**References**

[1]  Tomlinson G R: Recent Development in Particle Dampers, 6th National Turbine Engine High Cycle Fatigue Conference, 5-8 March 2001, Jacksonville, Florida

[2]  Liu W, Tomlinson G R and Worden K: Nonlinearity Study of Particle Dampers, ISMA 2002, International Conference on Noise and Vibration Engineering, 16 – 18, Sept. 2002, Leuven

[3]  Saluena C, Esipov S E, Rosenkranz D and Panossian H V: On Modelling of Arrays of Passive Granular Dampers, Proc. SPIE vol.3672, 32-42, 1999

[4]  Flower B, Flint E and Olson S: Design Methodology for Particle Damping, Presented at the SPIE Conference on Smart Structures and Materials, Newport Beach, CA, March 4-8, 2001. Paper # 4331-20

[5]  Saeki M: Impact Damping with Granular Materials in a Horizontally Vibrating System, Journal of Sound and Vibration, 251(1), 153-161, 2002

[6]  Duran J: Sands, Powders, and Grains, An Introduction to the Physics of Granular Materials, Springer-Verlag, 1999, ISBN0-387-98656-1

[7]  Oda M and Iwashita K: Mechanics of Granular Materials, An Introduction, A A Balkema Publisher, Rotterdam, 1999

[8]  Ovarlez G, Fond  C and Clement  E: A Giant Overshoot Effect in the Janssen Granular Column,   http://arxiv.org/PS_cache/cond-mat/pdf/0212/0212228.pdf,   December, 2002

[9]  Herrmann H J, Hovi J P and Luding S: Physics of Dry Granular Media, Kluwer Academic Publishers, Dordrecht Hardbound, ISBN 0-7923-5102-9 June 1998

[10] Petruccelli J D: Applied statistics for engineers and scientists, Upper Saddle River, N.J.: Prentice Hall; London: Prentice-Hall, 1999
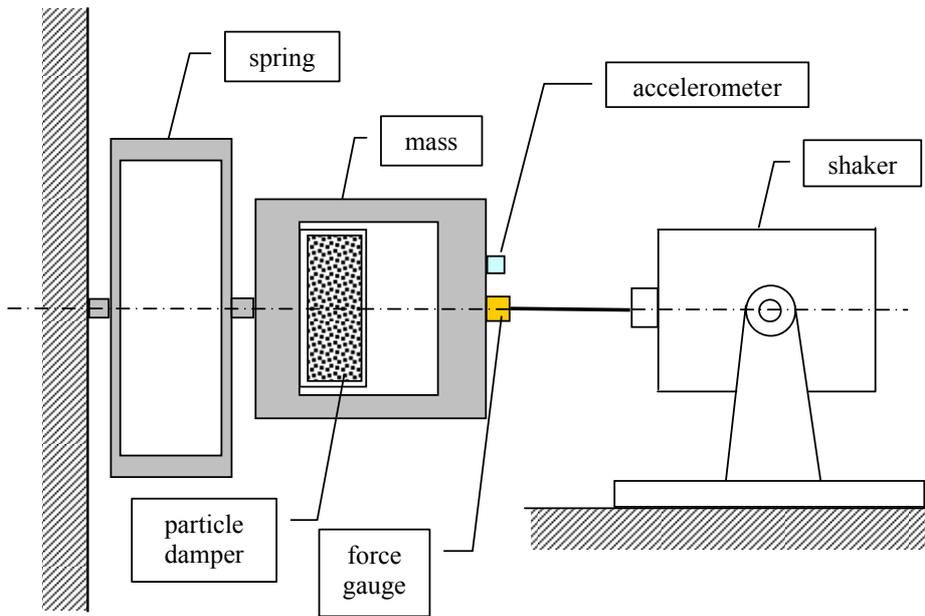
Figure 1: SDOF test rig
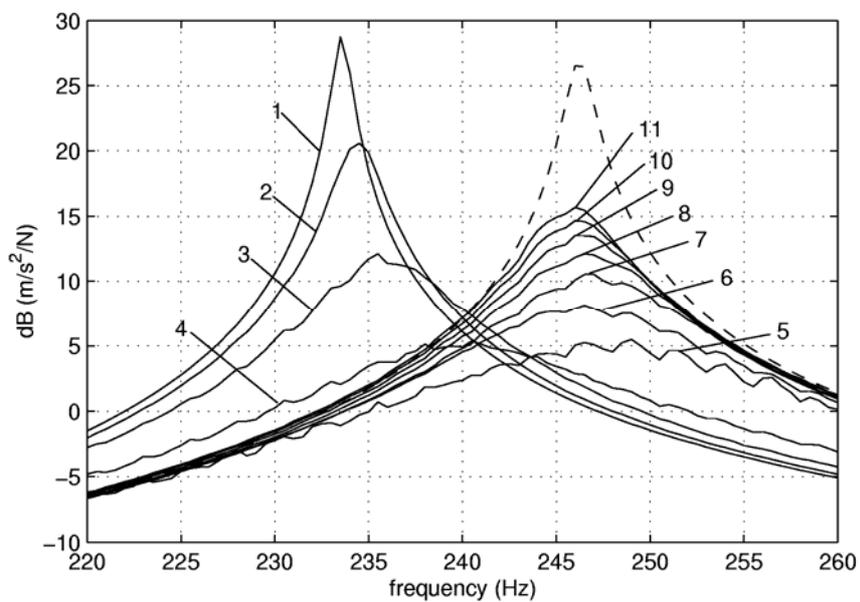


Figure 2: Dynamic behaviour of SDOF system with a particle damper ($\alpha = 0.4$)
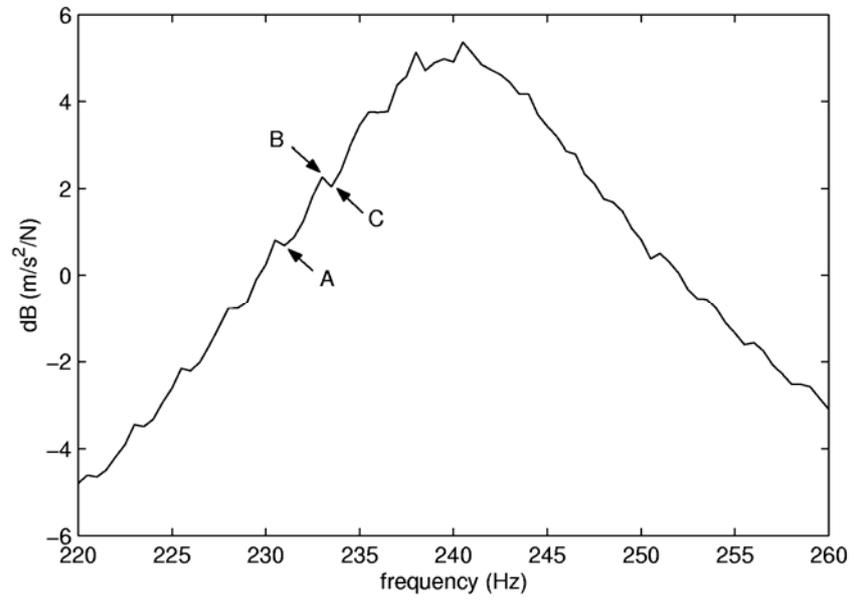
Figure 3: Demonstration of friction: stick-slip process
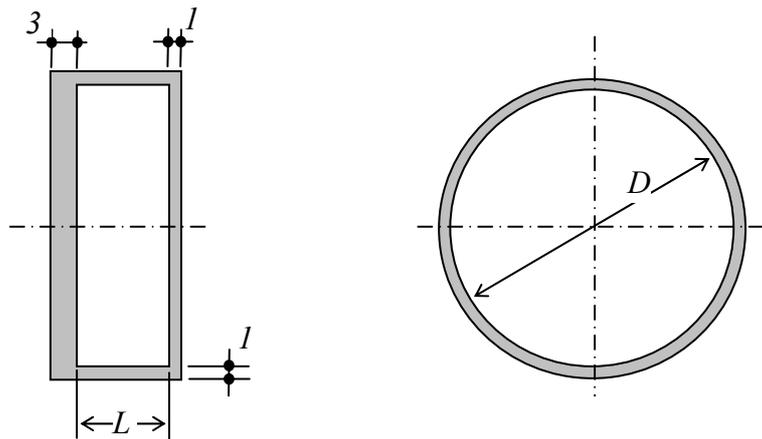


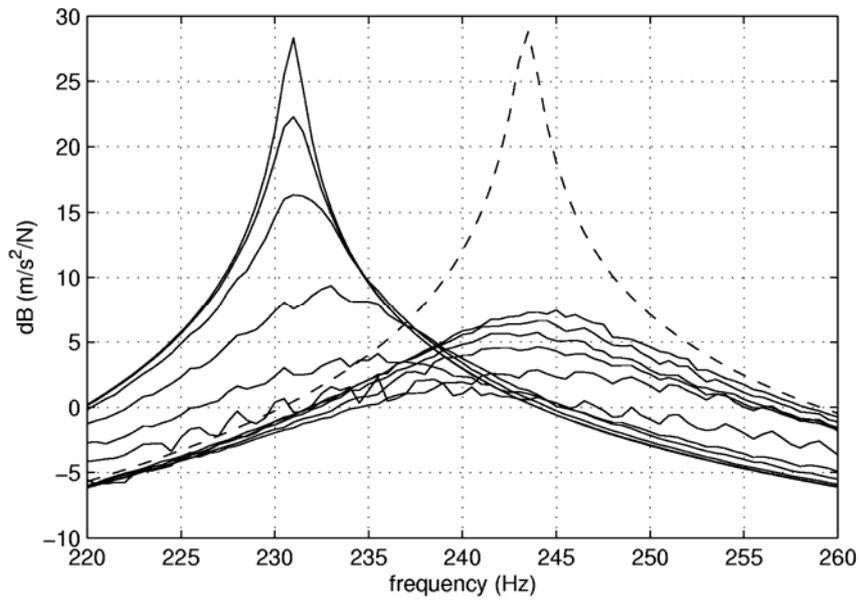Figure 4: Design of cavity (dimensions in *mm*)

Figure 5: FRFs of particle damper with $\alpha = 0.2$
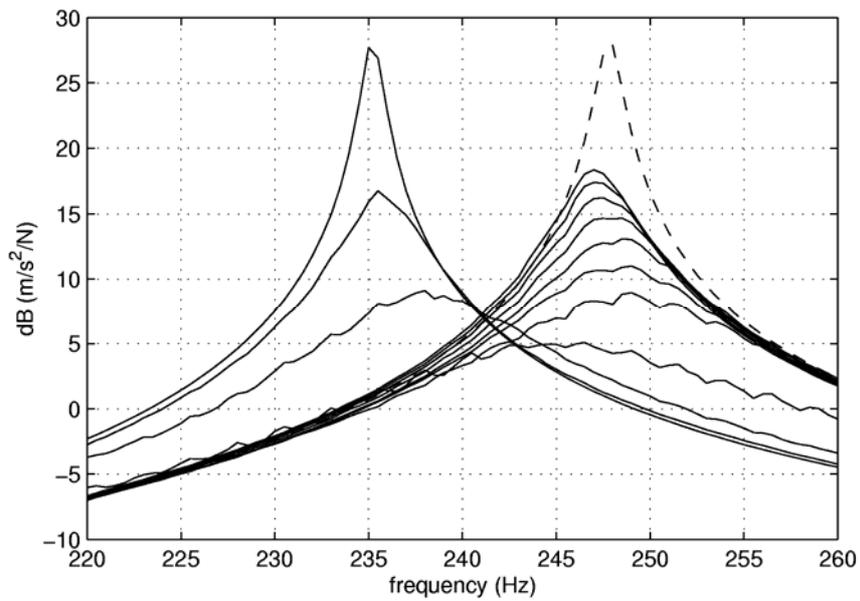


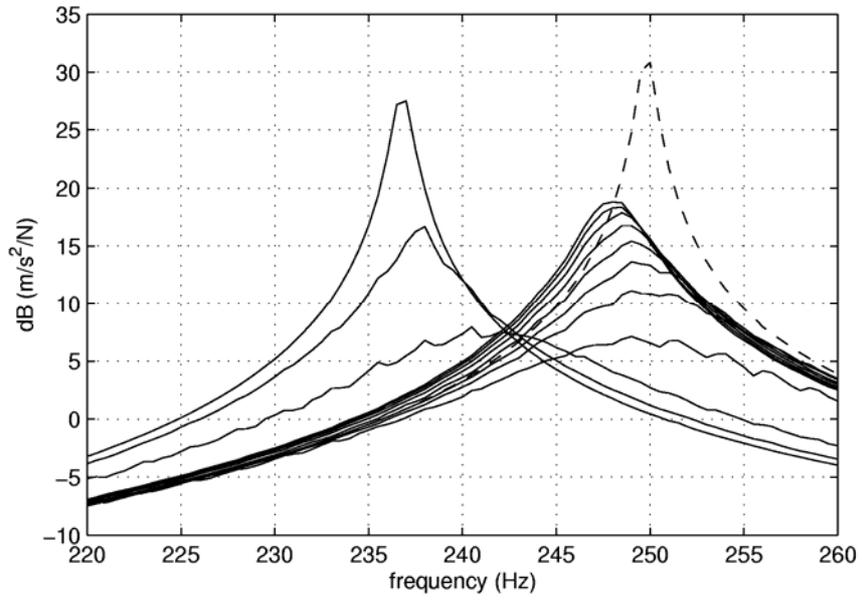Figure 6: FRFs of particle damper with $\alpha = 0.6$

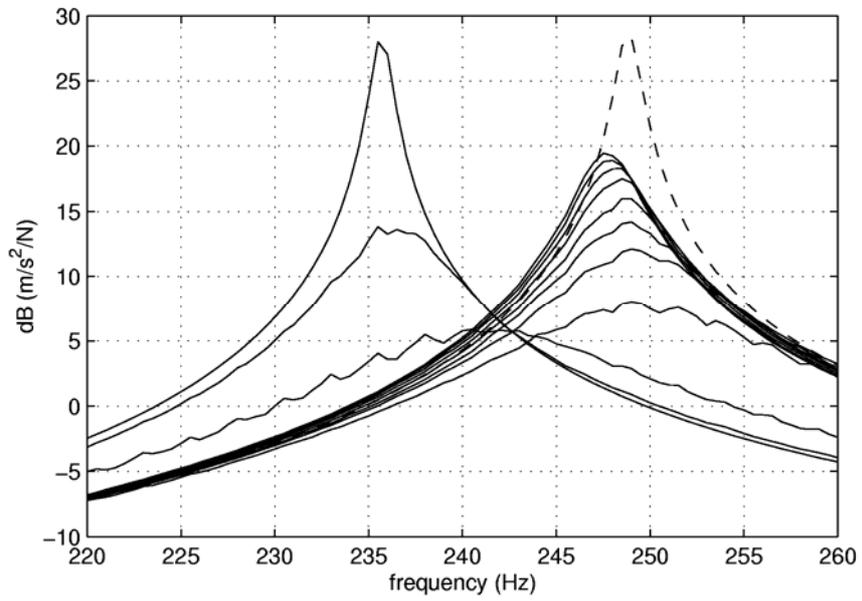Figure 7: FRFs of particle damper with $\alpha = 0.8$



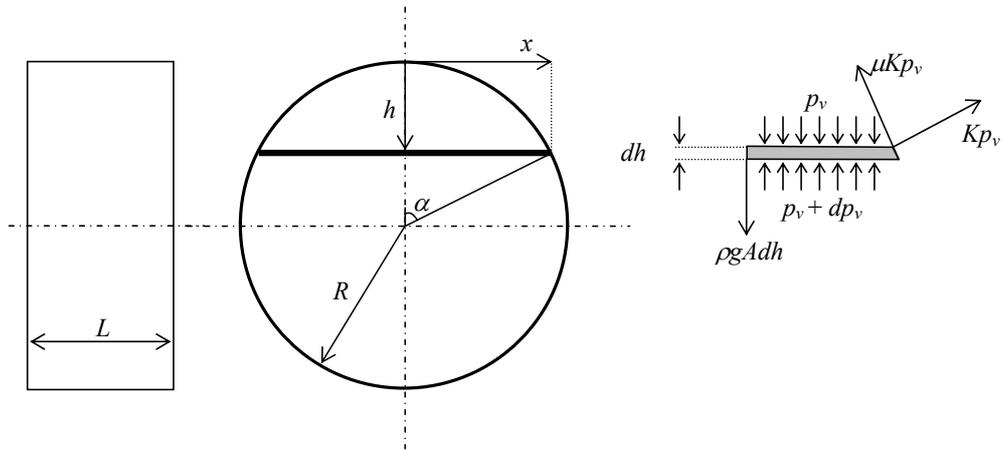Figure 8: FRFs of particle damper with $\alpha = 1.0$
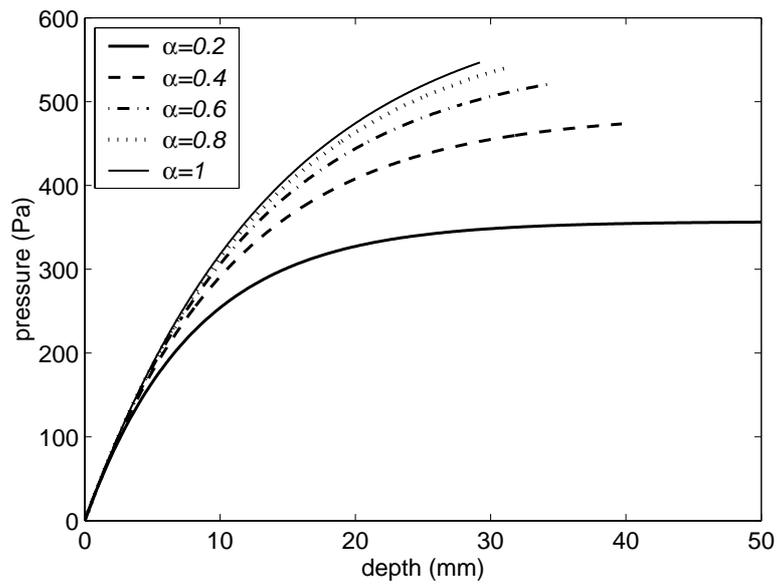
Figure 9: Pressure distribution model cylindrical dampers



Figure 10: Static pressure distribution of five different particle dampers
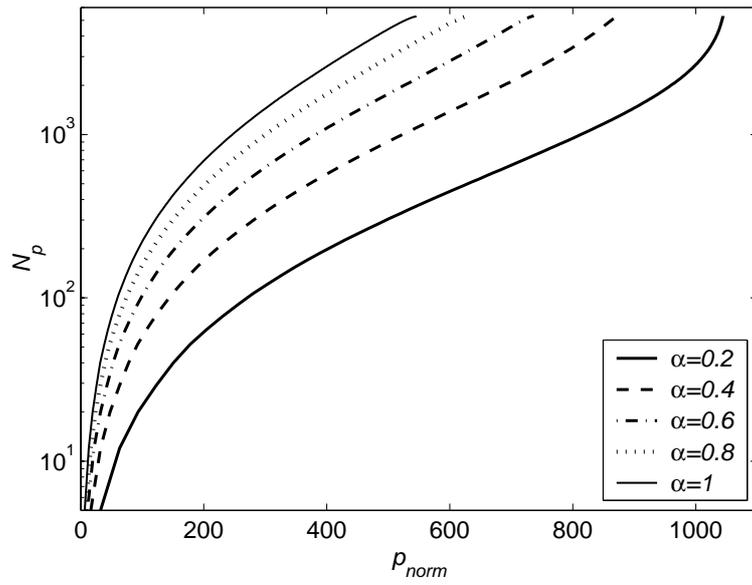
Figure 11: Number of particles $N_p$ against normalised pressure distribution, $p_{norm}$
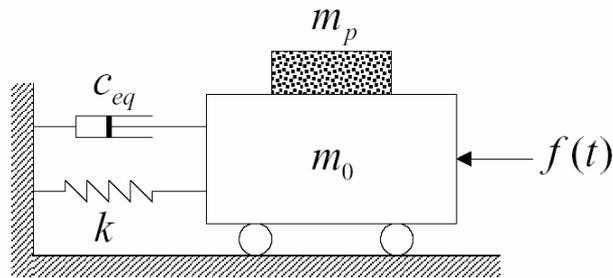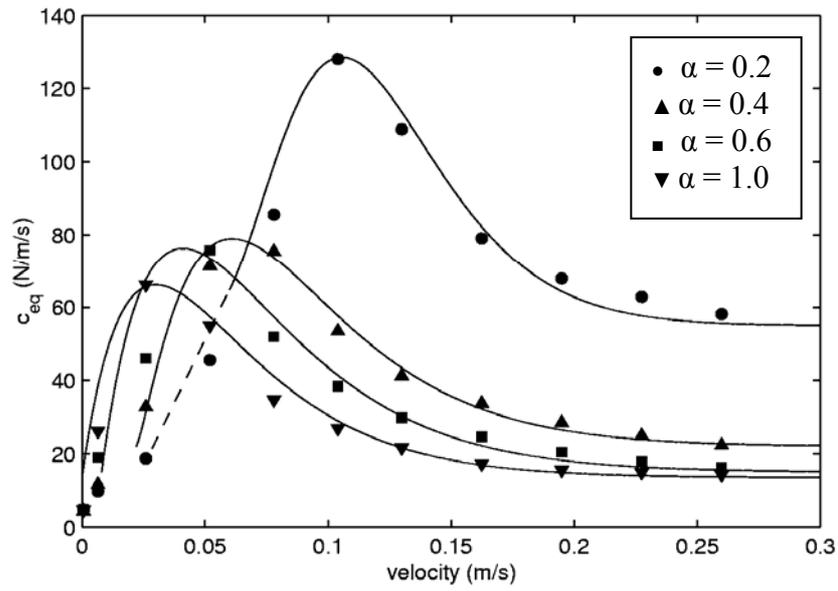


Figure 12: SDOF model

Figure 13: Curve fits of the equivalent damping coefficients as a function of the

velocity from Equation (11)

Table 1. Dimensions of PDs used

| α | 0.2 | 0.4 | 0.6 | 0.8 | 1.0 |
|---|---|---|---|---|---|
| D (*mm*) | 50.0 | 39.7 | 34.7 | 31.5 | 29.2 |
| L (*mm*) | 10.0 | 15.9 | 20.8 | 25.2 | 29.2 |
| Volume (*mm³*) | 19635 | 19682 | 19670 | 19639 | 19554 |

Table 2. Parameters of the nonlinear damping model for Equation (11)

| α | γ | β | μ | A | B |
|---|---|---|---|---|---|
| 0.2 | 5.1 | 0.016 | 0.040 | 6.1 | 55.0 |
| 0.4 | 2.3 | 0.030 | 0.022 | 5.5 | 22.0 |
| 0.6 | 2.0 | 0.032 | 0.008 | 5.2 | 15.0 |
| 1.0 | 2.0 | 0.033 | 0.000 | 4.3 | 13.5 |